IJMMM International Journal of Minerals, Metallurgy and Materials 矿物冶金与材料学报（英文版）

Performance and electromagnetic mechanism of radar- and infrared-compatible stealth materials based on photonic crystals

Yanming Liu, Xuan Yang, Lixin Xuan, Weiwei Men, Xiao Wu, and Yuping Duan

Cite this article as:
Yanming Liu, Xuan Yang, Lixin Xuan, Weiwei Men, Xiao Wu, and Yuping Duan, Performance and electromagnetic mechanism of radar- and infrared-compatible stealth materials based on photonic crystals, *Int. J. Miner. Metall. Mater.*, 32(2025), No. 3, pp. 710-717. https://doi.org/10.1007/s12613-024-2986-5

View the article online at SpringerLink or IJMMM Webpage.

INTERNATIONAL JOURNAL OF
Minerals, Metallurgy and Materials

Volume 32, Number 3, March 2025
Page 710

Research Article https://doi.org/10.1007/s12613-024-2986-5

Performance and electromagnetic mechanism of radar- and infrared-compatible stealth materials based on photonic crystals

Yanming Liu[1,2], *Xuan Yang*[1,2], *Lixin Xuan*[1,2], *Weiwei Men*[1,2], *Xiao Wu*[1,2], *and Yuping Duan*[3)✉]

1) AVIC Research Institute for Special Structures of Aeronautical Composite, Ji'nan 250023, China
2) Aviation Key Lab of Science and Technology on High Performance Electromagnetic Windows, Ji'nan 250023, China
3) Key Laboratory of Solidification Control and Digital Preparation Technology (Liaoning Province), School of Materials Science and Engineering, Dalian University of Technology, Dalian 116085, China
(Received: 22 May 2024; revised: 1 August 2024; accepted: 8 August 2024)

Abstract: Traditional stealth materials do not fulfill the requirements of high absorption for radar waves and low emissivity for infrared waves. Furthermore, they can be detected by various technologies, considerably threatening weapon safety. Therefore, a stealth material compatible with radar and infrared was designed based on the photonic bandgap characteristics of photonic crystals. The radar stealth layer (bottom layer) is a composite of carbonyl iron/silicon dioxide/epoxy resin, and the infrared stealth layer (top layer) is a 1D photonic crystal with alternately and periodically stacked germanium and silicon nitride. Through composition optimization and structural adjustment, the effective absorption bandwidth of the compatible stealth material with a reflection loss of less than −10 dB has reached 4.95 GHz. The average infrared emissivity of the proposed design is 0.1063, indicating good stealth performance. The theoretical analysis proves that photonic crystals with this structural design can produce infrared waves within the photonic bandgap, achieving high radar wave transmittance and low infrared emissivity. Infrared stealth is achieved without affecting the absorption performance of the radar stealth layer, and the conflict between radar and infrared stealth performance is resolved. This work aims to promote the application of photonic crystals in compatible stealth materials and the development of stealth technology and to provide a design and theoretical foundation for related experiments and research.

Keywords: microwave absorption; infrared stealth; photonic crystal; compatible stealth

1. Introduction

With the rapid development of intelligent and complex detection technologies [1–3], ensuring the safety of weapons and equipment has become increasingly difficult [4–5]. The combined use of various detection methods on the battlefield has promoted the development of stealth technology toward compatible stealth [6–7]. Radar and infrared detection methods are the most common [8]. Radar stealth requires strong electromagnetic wave absorption, and materials should exhibit low reflection and high electromagnetic wave absorption [9]. Meanwhile, the materials for infrared stealth should exhibit high reflectivity and low emissivity for electromagnetic waves [10–11]. These two stealth mechanisms are in conflict with each other and incompatible within the same material [6,12], considerably threatening the stealth and survival of weapon equipment. Thus, endowing stealth materials with applicability in radar and infrared stealth is a challenge that impedes the development of multiband compatible stealth technologies [13].

Composites can be endowed with radar and infrared stealth properties via ball milling and surface modification [14]. Lv *et al.* [15] prepared a flaky Fe/Al-mixed stealth material with an effective absorption bandwidth of 1.7 GHz, reflection loss of less than −10 dB, and infrared emissivity as low as 0.15. Lu *et al.* [16] prepared MWNT/$Zn_{0.96}Co_{0.04}O$ composite nanofibers with an effective absorption bandwidth of 4 GHz and an infrared emissivity of 0.61. By coating multiwalled carbon nanotubes with polyamide, Pan *et al.* [17] prepared a stealth material with a maximum reflection loss of −20.65 dB at 9.7 GHz, an effective absorption bandwidth of 3.2 GHz, and infrared emissivity up to 0.503 in the 8–14 μm band. These results show that achieving good radar and infrared stealth performances using a single material is difficult owing to different and contradictory stealth mechanisms [18]. Considering this limitation, this work designs a double-layer composite material by adding an infrared stealth layer to the surface of radar stealth materials to achieve compatible stealth capabilities.

Infrared stealth requires the target to have low emissivity in the infrared atmospheric windows in the bands of 3–5 and 8–14 μm. Kirchhoff's law [19] states that for an opaque target unit, the emissivity (ε) and reflectivity (r) are related as follows:

✉ Corresponding author: Yuping Duan E-mail: duanyp@dlut.edu.cn

$$\varepsilon + r = 1 \quad (1)$$

This formula shows that reflectivity and emissivity are interdependent and that a low emissivity requirement for infrared stealth can be achieved by adjusting the reflectivity of the material [20]. Photonic crystals are artificial optical microstructured materials [21], whose optical refractive index changes regularly with periodic changes in their structure, resulting in the formation of photonic bandgaps [22]. With the use of a structural design, electromagnetic waves in certain frequency bands can be completely reflected (or transmitted) into the photonic bandgap [23–24]. When a photonic bandgap is designed to encompass the infrared atmospheric window, the photonic crystals exhibit high reflectivity and low emissivity for infrared radiation; these characteristics can be exploited to achieve infrared stealth. Zhang and Lv [25] prepared 1D Ge/TiO_2 photonic crystals using optical coating technology, and the average emissivity of these crystals in the 8–14 μm band was as low as 0.202. Zhang *et al.* [26] designed and prepared opal photonic crystals containing SiO_2 microspheres whose bandgap could reach 1.9 μm. Photonic crystals can only prevent electromagnetic waves within the photonic bandgap from entering the material. Hence, they do not affect the propagation of electromagnetic waves with other frequencies and wavelengths. Therefore, materials with a specially designed structure that can exhibit low infrared emissivity and high transmittance for radar waves are required. When used in conjunction with radar stealth materials, they can absorb radar waves to achieve compatible stealth.

On the basis of the aforementioned mechanisms, photonic crystals have been designed using germanium (refractive index = 4.0) and silicon nitride (refractive index = 2.0) as raw materials to cooperate with traditional radar stealth materials. Wide photonic bandgaps have been observed owing to the large differences in refractive index between these materials, reducing the infrared emissivity via total reflection in the infrared band. Photonic crystals do not affect electromagnetic wave propagation within the nonphotonic bandgap; therefore, infrared stealth can be achieved without affecting radar stealth performance. As a semiconductor material with excellent performance, germanium is widely used in electronic devices [27] and is often employed as a high-refractive-index material for photonic crystals. As a ceramic material with excellent comprehensive properties, silicon nitride is widely used in microelectronics, solar cells, and other fields [28]; however, research on its stealth, particularly infrared stealth, is limited. In general, the wave transmission capability of silicon nitride [29] minimizes the loss in electromagnetic wave propagation and contributes to improving compatible stealth performance. Compared with some commonly used materials for preparing photonic crystals, such as ZnS and TiO_2, silicon nitride has a lower density and better mechanical properties, which renders it suitable for designing compatible stealth materials that can satisfy the requirements of "thin, light, wide, and strong" for suitable applications. In this study, the top infrared stealth layer was designed based on the optical characteristics of a 1D photonic crystal, and the bottom radar stealth layer was designed and optimized based on the effective medium theory. The stealth material obtained by combining these two layers was simulated and found to have an effective absorption bandwidth of less than 0.4% and a low infrared emission bandwidth of nearly 0.1. This result indicates a balanced performance between the infrared and radar stealth properties. The structures designed in this study effectively resolve the compatibility issue between radar and infrared stealth mechanisms. This study provides a new concept for designing compatible stealth materials and a theoretical basis for research on compatible stealth technologies for electromagnetic waves across other frequency bands.

2. Design principle

The radar/infrared-compatible stealth material designed in this study comprises two layers. The material design scheme is shown in Fig. 1. The top layer is a periodic 1D photonic crystal formed by alternately stacked Ge and Si_3N_4 layers. Owing to its photonic bandgap, the photonic crystal exhibits high reflectivity and low emissivity for infrared waves, en-

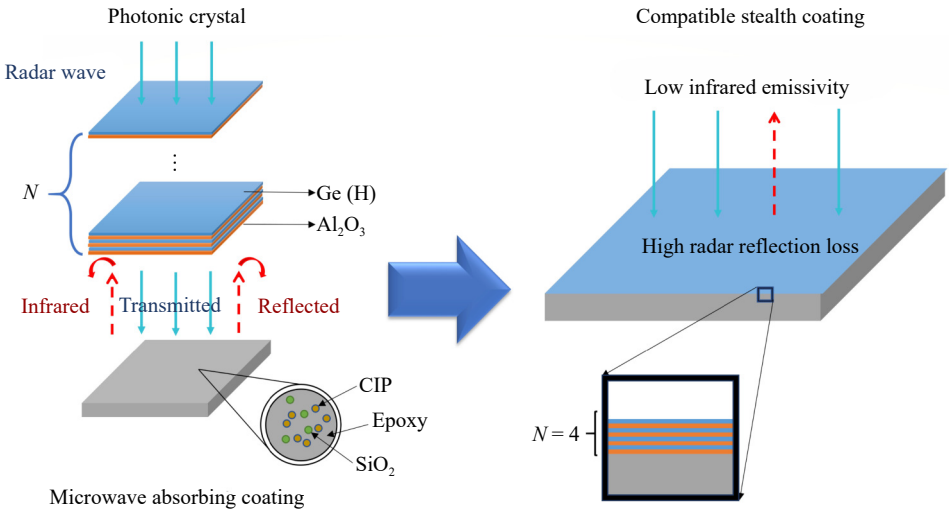

Fig. 1. Schematic of compatible stealth materials.

abling it to achieve infrared stealth. Moreover, this crystal has high transmittance for radar waves, allowing radar waves to easily enter its bottom layer. The bottom layer is a radar stealth material composed of carbonyl iron powder (CIP), silicon dioxide (SiO_2), and epoxy resin. According to the effective medium theory, the electromagnetic parameters of a material can be adjusted using the composition ratio to achieve a satisfactory radar-absorbing performance. The photonic crystal on the top layer and the absorbing material on the bottom layer work together to achieve low infrared emissivity without compromising the absorption performance. This collaboration enhances material stealth performance.

The top photonic crystal layer is a highly reflective film structure G|H(LH)^N|Air (G stands for the glass substrate, and H and L stand for the high- and low-refractive-index layers, respectively) with an optical thickness of a quarter of the central wavelength. The number of periods is N, and the maximum reflectivity of the central wavelength under the condition of normal incidence can be calculated as,

$$R = \left[\frac{1-(n_1/n_2)^N(n_1^2/n_0)}{1+(n_1/n_2)^N(n_1^2/n_0)}\right]^2 \tag{2}$$

where N, n_1, n_2, and n_0 represent the number of periods, refractive indices of the high-refractive index, low-refractive index, and base layers, respectively. This formula shows that reflectivity is related to the refractive index ratios of the high- and low-refractive-index layers and the number of periods. The greater the refractive index ratio and the number of periods, the greater the reflectivity of the film. Therefore, germanium and alumina with a large refractive index are selected to design photonic crystals aimed at the infrared atmospheric window in the 8–14 μm band. Their infrared stealth performance was optimized by adjusting their periods. The photonic bandgap of the as-designed photonic crystals was in the center of the 8–14 μm band. Radar waves (2–18 GHz) can be completely transmitted inside the photonic crystals without affecting the absorption performance of the material.

The radar stealth layer at the bottom is composed of carbonyl iron (density, 3.0 g/cm^3), SiO_2 (density, 2.2 g/cm^3), and epoxy resin (density, 1.2 g/cm^3). CIP is a ferromagnetic absorber with good performance that can be mixed with an epoxy resin matrix to produce a good-absorbing material. As a wave-transparent material [30], silicon dioxide has a low permittivity and can thus improve the impedance matching of stealth materials, produce a channel effect [31], and help optimize the wave-absorbing performance of stealth materials. The effective medium theory focuses on the related electromagnetic properties of a composite containing a medium and dispersed particles. Different theories are used for different conditions: Maxwell–Garnett (M–G) theory describes dispersed microstructures, and Bruggeman and differential effective medium theories describe symmetrical microstructures and cascade microstructures, respectively [32]. In this study, carbonyl iron and silicon dioxide were dispersed in epoxy resin, and the obtained mixture conformed to the basic model of spherical particles embedded in a matrix according to the M–G theory. Therefore, the relevant electromagnetic parameters of the designed materials were calculated using the M–G theory. Assuming that the volume fraction of spherical particles is q, the effective permittivity (ε_e) and permeability (μ_e) of the mixed medium can be expressed as [33–34],

$$\varepsilon_e = \varepsilon_2 + \frac{3q(\varepsilon_1-\varepsilon_2)\varepsilon_2/(\varepsilon_1+2\varepsilon_2)}{1-q(\varepsilon_1-\varepsilon_2)\varepsilon_2/(\varepsilon_1+2\varepsilon_2)} \tag{3}$$

$$\mu_e = \mu_2 + \frac{3q(\mu_1-\mu_2)\mu_2/(\mu_1+2\mu_2)}{1-q(\mu_1-\mu_2)\mu_2/(\mu_1+2\mu_2)} \tag{4}$$

where ε_1, ε_2 and μ_1, μ_2 represent the permittivities and permeabilities of the spherical particles and matrix, respectively.

3. Results and discussion

3.1. Performance and mechanism analysis of radar stealth layer

The electromagnetic parameters of carbonyl iron were measured, microwave-absorbing materials with different composition ratios were designed, and simulations were performed. Table 1 lists the simulation tools and key parameters. The calculation results are shown in Fig. 2. Fig. 2(a) shows that the reflection loss peak of the material gradually shifts to a lower frequency with increasing mass fraction of carbonyl iron in the material. According to the effective medium theory, the permittivity and permeability of the material gradually increase with increasing carbonyl iron content. According to quarter-wave theory [35]:

$$f_m = \frac{nc}{4d\sqrt{|\varepsilon_r'||\mu_r'|}} \quad (n = 1,3,5\ldots) \tag{5}$$

where f_m represents the matching frequency, d represents the thickness of the absorbing material, c represents the speed of

Table 1. Simulation tools and design parameters

Design tool	Design parameter
High-frequency structure simulator (HFSS) simulation software for radar stealth layer	Base material: perfect electric conductor (pec); base size: 40 mm × 40 mm × 1.5 mm; materials: CIP, SiO_2, epoxy; material size: 40 mm × 40 mm × 1 mm; environmental conditions: vacuum; environmental scope: 40 mm × 40 mm × 40 mm; incentive mode: FloquetPort; analysis method: sweep; scanning frequency band: 2–18 GHz; scanning step size: 0.2 GHz.
FDTD solutions (FDTD) simulation software for infrared stealth layer	Materials: Ge, Si_3N_4; bottom size: 40 mm × 40 mm; Ge layer thickness: 0.688 μm; Si_3N_4 layer thickness: 1.375 μm; boundary condition: periodic; type of light source: plane wave; test band: 8–14 μm; number of test points: 500.
HFSS simulation software for compatible stealth material	Materials: CIP, SiO_2, epoxy, Ge, and Si_3N_4; radar stealth material size: 40 mm × 40 mm × 1 mm; Ge layer size: 40 mm × 40 mm × 0.000688 mm; Si_3N_4 layer thickness: 40 mm × 40 mm × 0.001375 mm; scanning frequency band: 2–18 GHz; scanning step size: 0.2 GHz; other conditions are the same as those in radar stealth layer design.

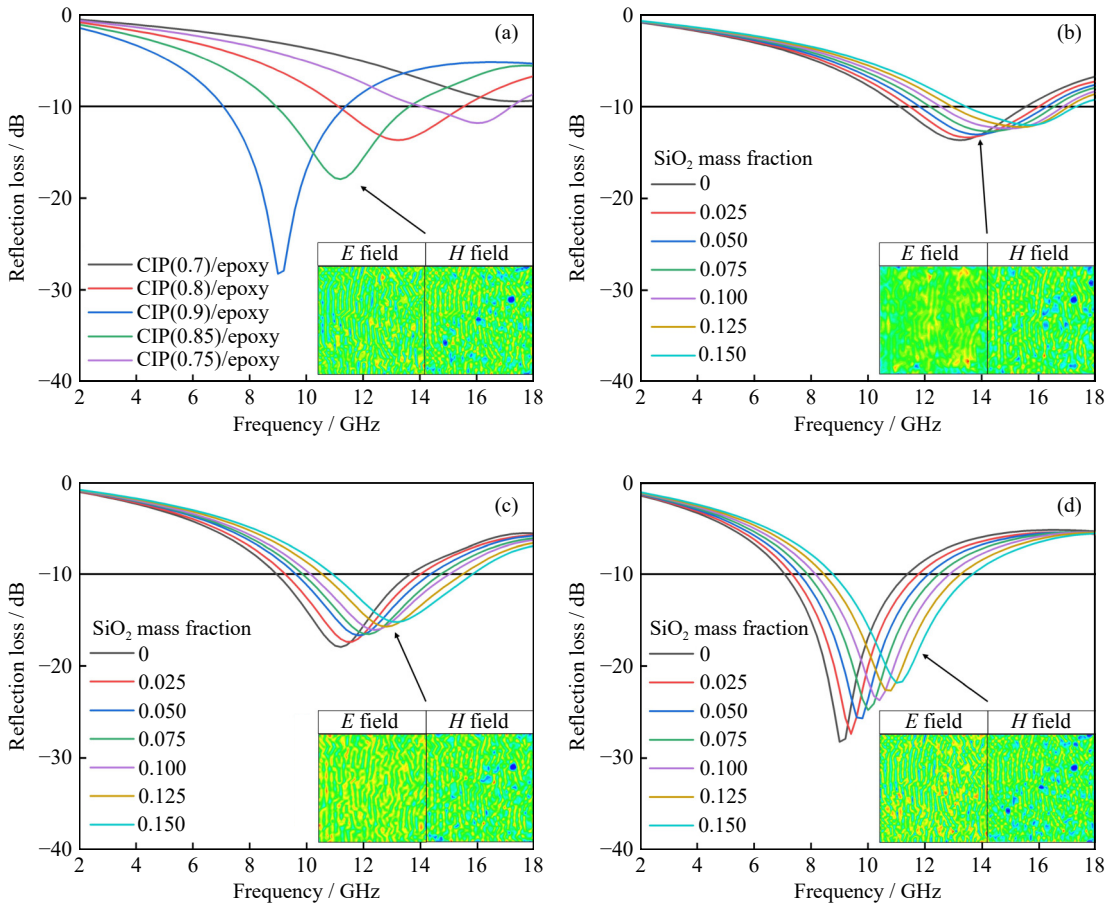

Fig. 2. Reflection loss curve of radar stealth materials and the distribution of electric (*E* field) and magnetic-field (*H* field) intensity when the effective absorption bandwidth is the widest: (a) radar-absorbing materials with different carbonyl iron mass fractions and radar stealth layer with different contents of silicon dioxide and carbonyl iron contents of (b) 0.8, (c) 0.85, and (d) 0.9, respectively.

light, ε_r' represents real part of the permittivity, and μ_r' represents real part of the permeability. With increasing carbonyl iron content, the matching frequency gradually moves from a high frequency to a low frequency, causing the reflection loss peak to move to a lower frequency.

The effective absorption bandwidth of the material initially increases and then decreases with increasing mass fraction of carbonyl iron. The content of carbonyl iron is critical to the material's permittivity, which in turn is pivotal in the impedance matching of the material [36]. Therefore, when the carbonyl iron content exceeds a certain threshold, the microwave absorption performance of the material decreases. When the mass fraction of carbonyl iron was 0.85, the material exhibited the best wave-absorbing performance with an effective absorption bandwidth of 4.72 GHz and a reflection loss reaching a peak of −18.0 dB at 11.2 GHz.

Absorbing materials with carbonyl iron mass fractions of 0.8, 0.85, and 0.9 were selected and added with SiO_2 (the SiO_2 addition amount cannot be large; therefore, the upper limit of SiO_2 mass fraction was controlled to be 0.15 to ensure the accuracy of the simulation results) to further optimize the absorption performance of the radar stealth layer. The changes in the absorption performance of the materials with added amounts of silicon are shown in Fig. 2(b)–(d). After SiO_2 was added to the material, the reflection loss peak shifted to a higher frequency. When the mass fraction of carbonyl iron was 0.8 (Fig 2(b)) and 0.85 (Fig 2(c)), the effective absorption bandwidth of the material initially increased and then decreased with increasing SiO_2 mass fraction, reaching maximum widths of 4.54 and 4.97 GHz when the mass fractions of SiO_2 were 0.025 and 0.125, respectively. When the content of carbonyl iron was 0.8 or 0.85, the decrease in permittivity and permeability caused by SiO_2 addition considerably influenced the microwave absorption performance of the material. When the SiO_2 content exceeded a threshold value, the microwave absorption ability of the material worsened. When the mass fraction of carbonyl iron was 0.9, the effective absorption bandwidth of the material gradually increased with the mass fraction of SiO_2 increasing to 0.15. Accordingly, the maximum absorption bandwidth reached 4.92 GHz.

Fig. 3 shows an enhancement in the electric and magnetic field strengths, dielectric loss capacity, and magnetic loss capacity of the absorbing material after the addition of 12.5wt% SiO_2 and 85wt% carbonyl iron. As a result, the absorbing performance of the material is improved. According to the effective medium theory, SiO_2 addition decreases the permittivity and permeability of the composites, with the permittivity decreasing more considerably than the permeability. According to the impedance-matching formula [37]:

$$Z_{in} = Z_0 \eta \tanh(\gamma d) \tag{6}$$

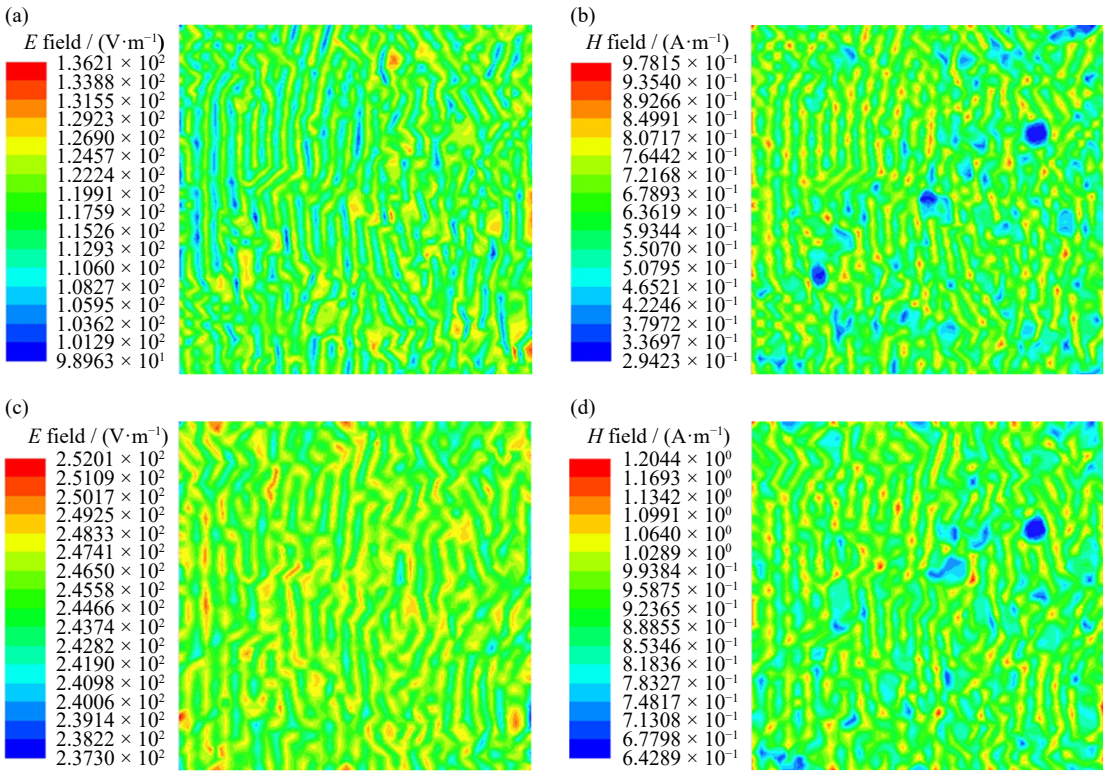

Fig. 3. (a) Distribution of electric and (b) magnetic fields on the surface of the absorbing material with 85wt% carbonyl iron and (c) distribution of electric and (d) magnetic fields on the surface of the absorbing material with 85wt% carbonyl iron and 12.5wt% SiO_2.

$$\eta = \sqrt{\frac{\mu_r}{\varepsilon_r}} = \sqrt{\frac{\mu_r' - j\mu_r''}{\varepsilon_r' - j\varepsilon_r''}} \tag{7}$$

$$\gamma = j\frac{\omega}{c}\sqrt{\mu_r\varepsilon_r} = j\frac{2\pi f}{c}\sqrt{(\mu_r' - j\mu_r'')(\varepsilon_r' - j\varepsilon_r'')} \tag{8}$$

where Z_{in}, Z_0, η, γ, d, ε_r'', and μ_r'' represent the input wave impedance, the impedance of free space, characteristic impedance, propagation constant, thickness of the material, imaginary part of the permittivity, and imaginary part of the permeability, respectively. With decreasing permittivity, the input wave impedance of the material approaches that of air. Thus, SiO_2 addition can improve the impedance matching of the material, allowing electromagnetic waves to easily enter the material and escape further. As a wave-transmitting material, SiO_2 can also optimize the wave-transmitting rate of composites and broaden the frequency range of effective absorption, considerably improving and optimizing the wave-absorbing ability of materials. Therefore, materials with 12.5wt% SiO_2 and 85wt% carbonyl iron exhibit the best absorbing performance, with the maximum effective absorbing bandwidth reaching 4.97 GHz.

3.2. Reflectivity and photonic bandgap of infrared stealth photonic crystals

The top layer of the compatible stealth material is an infrared stealth material based on a 1D photonic crystal. According to Eq. (2), the reflectivity of photonic crystals gradually increases with increasing number of periods (N). In theory, the reflectivity can be increased to 1 by increasing the number of periods. However, indefinitely increasing the number of periods is impractical because the maximum number of photonic crystal periods is limited by the manufacturing process. Therefore, the number of periods (N) in which the Ge and Si_3N_4 layers of the photonic crystals were alternately stacked was selected to be 2, 3, 4, and 5, and the wavelength–reflectivity curves in the 8–14 μm band were obtained and compared (Fig. 4).

A comparison of the reflectivity curves of photonic crystals with different periods revealed that with the increase in the periods, the boundary between the photonic and non-photonic bandgap becomes increasingly clear, and the width of the photonic bandgap tends to be stable. The reflectivity at the photonic bandgap gradually increased, reaching above 0.75 at $N = 2$. In addition, the photonic bandgap is almost 1 when $N = 5$, which is close to the total reflection of incident infrared waves. When the infrared ray propagates through the

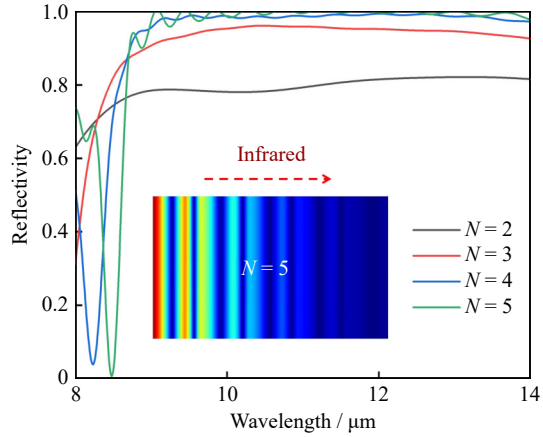

Fig. 4. Reflectance curve and energy-field distribution of Ge/Si_3N_4 photonic crystals with different periods.

periodic structure of Ge/Si_3N_4, it falls into the photonic bandgap and cannot propagate further due to the influence of the periodically changing refractive index [38]. This phenomenon leads to the high reflectivity of the Ge/Si_3N_4 photonic crystal to infrared rays, thus reducing the emissivity and realizing infrared stealth. According to the energy-field distribution diagram of the incident infrared rays, the surface energy of the photonic crystal is relatively high, and its internal energy gradually decreases along the direction of incidence of the infrared rays. This finding also demonstrates that the infrared rays in the band of 8–14 μm fall within the photonic bandgap, preventing them from propagating in the photonic crystal. Thus, high reflectivity and low emissivity close to total reflection are achieved.

According to the calculation of the average reflectivity and emissivity and the comprehensive analysis of the energy-field distribution, the designed photonic crystal film has the widest photonic bandgap and the best infrared stealth performance when N = 3. The average reflectivity was 0.8937, and the average emissivity was reduced to 0.1063. These results satisfy the performance requirements for effective low infrared stealth.

3.3. Performance of compatible stealth materials

On the basis of the above results, a simulation was performed by combining radar stealth materials and 1D photonic crystals with N = 3. The radar transmittances of these photonic crystals were tested to explore their influence on the microwave absorption properties of the materials.

The simulation results showed that the reflection loss peak shifts to a lower frequency after the photonic crystals are added to the radar stealth materials to produce compatible stealth materials. The effective absorption bandwidth changes from 4.97 to 4.95 GHz, indicating that the absorption performance remains unchanged. The comparison and analysis (Fig. 5) showed that the addition of the 1D photonic crystals reduces the surface electric and magnetic-field strengths of the material. However, the photonic crystals did not weaken the radar waves. According to the radar wave transmission curve of the photonic crystals (Fig. 5(b)), the transmittance of radar waves to the photonic crystals exceeds 99.93% in the frequency band of 2–18 GHz, indicating that adding photonic crystals to the surface of the radar stealth material has a minimal effect on the latter's performance. Meanwhile, the transmittance of the photonic crystals for low-frequency radar waves is higher than that for high-frequency radar waves, demonstrating that the reflected loss peak of the photonic crystals moves slightly toward lower frequencies after being added to compatible stealth materials. Given that the addition of a 1D photonic crystal infrared stealth film to the bottom radar stealth material has a minimal influence on radar absorption performance, a photonic crystal is adopted to improve the stealth performance of the material. The optical thickness of the Ge and Si_3N_4 layers in this study was set to be 1/4 of the central wavelength (11 μm) so that the total reflection was in the 8–14 μm band. Meanwhile, the average reflectivity of electromagnetic waves in other wavelength ranges is extremely small and hence negligible, ensuring that the absorption performance of the materials is not weakened and that the compatible stealth performances of radar and infrared waves are achieved.

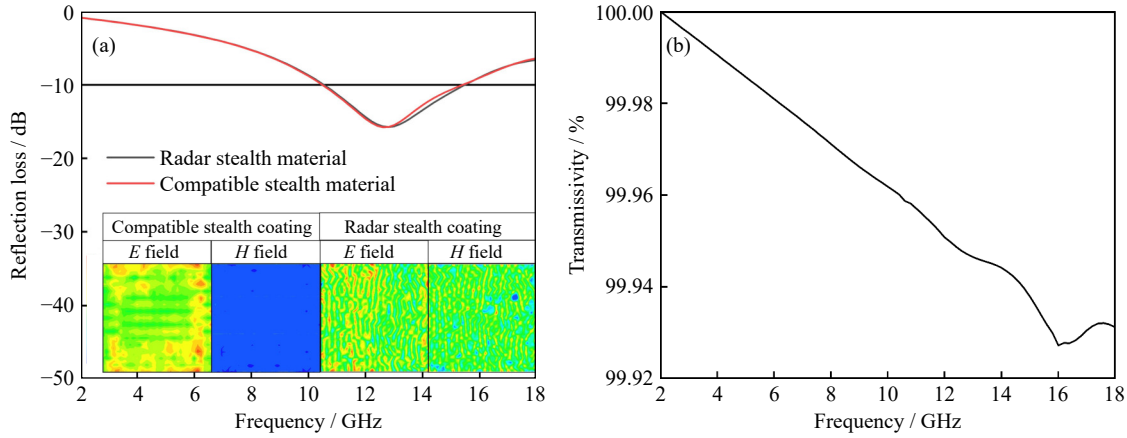

Fig. 5. (a) Comparison of the reflection loss curve and electric and magnetic fields between the radar stealth material with 85wt% carbonyl iron and 12.5wt% silica and the photonic crystal with period number N = 3 and (b) radar transmittance curve of the photonic crystals with period number N = 3.

The radar stealth performance of the optimized compatible stealth material is marginally influenced by the top photonic crystal, and the change in effective absorption bandwidth is less than 0.4%. The average infrared emissivity of the material was 0.1063, which meets the requirements for compatible stealth. As a low-refractive-index material, silicon nitride is used to design 1D photonic crystals with excellent performance.

4. Conclusion

The effective absorption bandwidth of the carbonyl iron/epoxy resin absorbing material reached 4.72 GHz when 85wt% carbonyl iron was added, and the maximum effective absorption bandwidth of the radar stealth material reached 4.97 GHz when 12.5wt% SiO_2 was further added. When the period number of the alternately stacked Ge and Si_3N_4 layers

was $N = 3$, the designed photonic crystal exhibited the best performance, and its surface electric- and magnetic-field distributions exerted the least influence on the absorption performance. A high transmittance of >99.93% for radar waves and an average infrared emissivity of 0.1063 were observed. The effective absorption bandwidth and infrared emissivity of the optimized compatible stealth material are 4.95 GHz and 0.1063, respectively, which leads to its low infrared emissivity and good absorption performance and balances its radar and infrared stealth to the maximum extent. The results of this study serve as a reference and guidance for the design of compatible stealth materials, and the selected Si_3N_4 material can be used for fabricating photonic crystals with broad application prospects in the field of multiband compatible stealth.

Acknowledgements

This work was supported by the National Natural Science Foundation of China (Nos. 52071053, U1704253, and 52103334).

Conflict of Interest

The authors declare that they have no conflicts of interest.

References

[1] L.L. Liang, X.Y. Yang, C. Li, *et al*., MXene-enabled pneumatic multiscale shape morphing for adaptive, programmable and multimodal radar–infrared compatible camouflage, *Adv. Mater.*, 36(2024), No. 24, art. No. 2313939.

[2] H. Luo, B.B. Ma, F. Chen, *et al*., Bimetallic oxalate rod-derived NiFe/Fe_3O_4@C composites with tunable magneto–dielectric properties for high-performance microwave absorption, *J. Phys. Chem. C*, 125(2021), No. 44, p. 24540.

[3] W.H. Gu, S.J.H. Ong, Y.H. Shen, *et al*., A lightweight, elastic, and thermally insulating stealth foam with high infrared–radar compatibility, *Adv. Sci.*, 9(2022), No. 35, art. No. 2204165.

[4] Z.Y. Zhou and J. Huang, Mixed design of radar/infrared stealth for advanced fighter intake and exhaust system, *Aerosp. Sci. Technol.*, 110(2021), art. No. 106490.

[5] Z.Y. Zhou, J. Huang, and J.J. Wang, Radar/infrared integrated stealth optimization design of helicopter engine intake and exhaust system, *Aerosp. Sci. Technol.*, 95(2019), art. No. 105483.

[6] Y. Wu, S.J. Tan, Y. Zhao, L.L. Liang, M. Zhou, and G.B. Ji, Broadband multispectral compatible absorbers for radar, infrared and visible stealth application, *Prog. Mater. Sci.*, 135(2023), art. No. 101088.

[7] X.L. Chen, C.H. Tian, Z.X. Che, and T.P. Chen, Selective metamaterial perfect absorber for infrared and 1.54 μm laser compatible stealth technology, *Optik*, 172(2018), p. 840.

[8] Z.G. Cheng, F. Zhao, X.K. Wang, X.D. Cai, X.J. Tang, and K. Han, Coaxial electrospinning fabrication and radar–infrared compatible stealth properties of $Zn_{0.96}Co_{0.04}O$ nanotubes, *J. Alloys Compd.*, 835(2020), art. No. 155368.

[9] C.L. Xu, B.K. Wang, M.B. Yan, *et al*., An optically transparent sandwich structure for radar–infrared bi-stealth, *Infrared Phys. Technol.*, 105(2020), art. No. 103108.

[10] L.P. Chen, Z.Y. Ren, X.M. Liu, K. Wang, and Q. Wang, Infrared–visible compatible stealth based on Al–SiO_2 nanoparticle composite film, *Opt. Commun.*, 482(2021), art. No. 126608.

[11] Q. Yuan, J.M. Jiang, Y.F. Li, *et al*., The compatible method of designing the transparent ultra-broadband radar absorber with low infrared emissivity, *Infrared Phys. Technol.*, 123(2022), art. No. 104114.

[12] Y. Zhu, L. Zhang, J. Wang, *et al*., Microwave–infrared compatible stealth via high-temperature frequency selective surface upon Al_2O_3–TiC coating, *J. Alloys Compd.*, 920(2022), art. No. 165977.

[13] Z.Q. Gao, Q. Fan, X.X. Tian, *et al*., An optically transparent broadband metamaterial absorber for radar–infrared bi-stealth, *Opt. Mater.*, 112(2021), art. No. 110793.

[14] M.Y. Shi, C. Xu, Z.H. Yang, *et al*., Achieving good infrared–radar compatible stealth property on metamaterial-based absorber by controlling the floating rate of Al type infrared coating, *J. Alloys Compd.*, 764(2018), p. 314.

[15] H.L. Lv, G.B. Ji, X.G. Li, *et al*., Microwave absorbing properties and enhanced infrared reflectance of FeAl mixture synthesized by two-step ball-milling method, *J. Magn. Magn. Mater.*, 374(2015), p. 225.

[16] S.B. Lu, Y. Meng, H.B. Wang, *et al*., Tailoring conductive network Zn@NPC@MWCNTs nanocomposites derived from ZIF-8 as high-performance electromagnetic absorber for the whole X-band, *Def. Technol.*, 23(2023), p. 189.

[17] W.L. Pan, M. He, X.H. Bu, *et al*., Microwave absorption and infrared emissivity of helical polyacetylene@multiwalled carbon nanotubes composites, *J. Mater. Sci. Mater. Electron.*, 28(2017), No. 12, p. 8601.

[18] Z.Y. Zhang, M.Z. Xu, X.F. Ruan, *et al*., Enhanced radar and infrared compatible stealth properties in hierarchical SnO_2@ZnO nanostructures, *Ceram. Int.*, 43(2017), No. 3, p. 3443.

[19] Z.M. Zhang, X.H. Wu, and C.J. Fu, Validity of Kirchhoff's law for semitransparent films made of anisotropic materials, *J. Quant. Spectrosc. Radiat. Transfer*, 245(2020), art. No. 106904.

[20] Z.C. Deng, Y.R. Su, W. Gong, X. Wang, and R.Z. Gong, Temperature characteristics of Ge/ZnS one-dimension photonic crystal for infrared camouflage, *Opt. Mater.*, 121(2021), art. No. 111564.

[21] S. Chen, L.Y. Guo, M.H. Ji, *et al*., Photonic crystal enhanced laser desorption and ionization substrate for detection of stress biomarkers under atmospheric pressure, *J. Mater. Chem. B*, 7(2019), No. 6, p. 908.

[22] A. Biswal, R. Kumar, C. Nayak, and S. Dhanalakshmi, Photonic bandgap characteristics of GaAs/AlAs-based one-dimensional quasi-periodic photonic crystal, *Optik*, 234(2021), art. No. 166597.

[23] S. Razi, F. Sepahi, and A.A. Saray, Graphene based photonic crystals including anisotropic defect layers with highly tunable optical responses in infrared frequency range, *Phys. B: Condens. Matter*, 597(2020), art. No. 412380.

[24] M. Heshmat and P.C.H. Li, Construction of an array of photonic crystal films for visual differentiation of water/ethanol mixtures, *ACS Omega*, 4(2019), No. 22, p. 19991.

[25] W.G. Zhang and D.D. Lv, Preparation and characterization of Ge/TiO_2 one-dimensional photonic crystal with low infrared-emissivity in the 8–14 μm band, *Mater. Res. Bull.*, 124(2020), art. No. 110747.

[26] L.C. Zhang, L.L. Qiu, W. Lu, *et al*., Preparation of opal photonic crystal infrared stealth materials, *Acta Phys. Sin.*, 66(2017), No. 8, art. No. 084208.

[27] T. Nagano, R. Hara, K. Moto, K. Yamamoto, and T. Sadoh, Improved carrier mobility of Sn-doped Ge thin films (≤20 nm) on insulator by interface-modulated solid-phase crystallization combined with surface passivation, *Mater. Sci. Semicond. Process.*, 165(2023), art. No. 107692.

[28] J. He and Y.C. Ke, Plasma-enhanced chemical vapor-deposited SiN and liquid-phase-deposited SiO_2 stack double-layer anti-re-

flection films for multi-crystalline solar cells, *Superlattices Microstruct.*, 122(2018), p. 296.

[29] M. Bouzidi, A.S. Alshammari, S. Soltani, *et al*., Correlation of structural and optical properties of AlGaN films grown on SiN-treated sapphire by MOVPE, *Mater. Sci. Eng. B*, 263(2021), art. No. 114866.

[30] L. Li, Y. Fang, Q. Xiao, Y.J. Wu, N. Wang, and X.M. Chen, Microwave dielectric properties of fused silica prepared by different approaches, *Int. J. Appl. Ceram. Technol.*, 11(2014), No. 1, p. 193.

[31] D. Szwagierczak, B. Synkiewicz, and J. Kulawik, Low dielectric constant composites based on B_2O_3 and SiO_2 rich glasses, cordierite and mullite, *Ceram. Int.*, 44(2018), No. 12, p. 14495.

[32] Y. Yang, Y. Yang, W. Xiao, C.P. Neo, and J. Ding, Shape-dependent microwave permeability of Fe_3O_4 nanoparticles: A combined experimental and theoretical study, *Nanotechnology*, 26(2015), No. 26, art. No. 265704.

[33] C. Guo, Z.H. Yang, S.L. Shen, J. Liang, and G.Y. Xu, High microwave attenuation performance of planar carbonyl iron particles with orientation of shape anisotropy field, *J. Magn. Magn. Mater.*, 454(2018), p. 32.

[34] N. Zhang, Y. Wang, P.Z. Chen, and W.X. Chen, A rational route towards dual wave-transparent type of carbonyl iron@SiO_2@heterogeneous state polypyrrole@paraffin composites for electromagnetic wave absorption application, *J. Colloid Interface Sci.*, 581(2021), p. 84.

[35] B.C. Wang, J.Q. Wei, Y. Yang, T. Wang, and F.S. Li, Investigation on peak frequency of the microwave absorption for carbonyl iron/epoxy resin composite, *J. Magn. Magn. Mater.*, 323(2011), No. 8, p. 1101.

[36] Y.P. Duan, Y. Liu, Y.L. Cui, G.J. Ma, and T.M. Wang, Graphene to tune microwave absorption frequencies and enhance absorption properties of carbonyl iron/polyurethane coating, *Prog. Org. Coat.*, 125(2018), p. 89.

[37] B.C. Wang, L.Y. Zhang, X. Zhao, *et al*., Unique dielectric dispersion induced ultra-broadband microwave absorption of tellurium doped black phosphorus nanoflakes/aramid nanofibers/carbonyl iron nanopowders ultra-lightweight aerogel, *Ceram. Int.*, 49(2023), No. 18, p. 30837.

[38] V. Pourmahmoud and B. Rezaei, Manipulation of Bragg and graphene photonic band gaps in one-dimensional photonic crystal containing graphene, *Optik*, 185(2019), p. 875.